macromol

MDPI

Article

Fabrication and Characterization of Collagen–Magnetic Particle Composite Microbeads for Targeted Cell Adhesion and Proliferation

Daichi Tanoshiri [1], Sakura Inoue [1], Shigehisa Aoki [2], Akira Kimoto [3], Yushi Oishi [1] and Takayuki Narita [1,*]

[1] Department of Chemistry and Applied Chemistry, Saga University, Saga 840-8502, Japan
[2] Department of Pathology and Microbiology, Saga University, Saga 849-8501, Japan
[3] Department of Electrical and Electronic Engineering, Saga University, Saga 849-8502, Japan
* Correspondence: naritat@cc.saga-u.ac.jp; Tel.: +81-952-28-8805

Abstract: The integration of the biocompatibility of collagen and the remote-control ability of magnetic elements serves as both a cell scaffold and an actuator. We studied the preparation, characterization, and potential applications of collagen–magnetic particle composite microbeads (CMPMBs). The interplay among collagen concentration, particle size, and surface roughness was found to influence cell adhesion and proliferation. Adsorption and desorption tests showed the reversible attachment of the particles to magnetic sheets, enabling precise spatial control and targeted cell delivery. The particles demonstrated their utility as cell carriers, supporting cell migration and proliferation. These findings showcase the potential of CMPMBs as a promising platform for advanced cell delivery and tissue regeneration applications. The ability to fine-tune particle properties and manipulate them using magnetic fields offers new possibilities for creating complex tissue constructs and controlling cellular behavior, which could contribute to the development of more effective regenerative therapies and tissue engineering approaches.

Keywords: collagen–magnetic particle composite microbeads; targeted cell delivery; collagen; scaffolds

Citation: Tanoshiri, D.; Inoue, S.; Aoki, S.; Kimoto, A.; Oishi, Y.; Narita, T. Fabrication and Characterization of Collagen–Magnetic Particle Composite Microbeads for Targeted Cell Adhesion and Proliferation. *Macromol* **2024**, *4*, 462–474. https://doi.org/10.3390/macromol4030027

Academic Editors: Dimitrios Bikiaris and Pradip K. Bhowmik

Received: 30 April 2024
Revised: 25 June 2024
Accepted: 2 July 2024
Published: 4 July 2024

1. Introduction

The extracellular matrix (ECM) plays a crucial role in regulating cellular functions and tissue regeneration [1–3]. In the fields of tissue engineering and regenerative medicine, there is growing interest in developing biomaterials that can effectively mimic the native ECM to promote cell adhesion, proliferation, and differentiation for improved therapeutic outcomes [4,5]. Scaffolds, in particular, are vital components that control key cellular processes, such as cell adhesion, migration, proliferation, and differentiation, through their chemical, topographical, and mechanical properties [6–8]. An ideal scaffold should replicate the unique structural and mechanical characteristics of the target tissue to enhance cell–matrix interactions and overall performance [9,10].

Collagen, as a major ECM component, has gained significant attention due to its exceptional biocompatibility and ability to support cell viability and adhesion [11–13]. Numerous studies have demonstrated the potential of collagen-based materials as cell delivery vehicles [12,14,15]. In parallel, magnetic particles are increasingly being explored in biomedical engineering for various applications, including cell separation [16], immunoassays [17], and drug delivery [18–20]. The unique physicochemical properties of submicron and nanometer-sized magnetic particles make them particularly advantageous for targeted drug delivery [21], cell separation [22], and cancer therapy [23,24].

The integration of magnetic particles with collagen has been studied for the development of cell scaffolds [25]. This composite cell scaffold not only controls cell orientation [26] but also allows for external manipulation of the cell microenvironment through magnetic fields. Thus, this synergistic combination has resulted in higher functional tissue regeneration in bones [27,28], tendons [26], and nerves [29]. The ability to remotely manipulate

magnetic particles in collagen gels provides new opportunities to non-invasively modulate the delivery and release of targeted drugs [30].

In this study, we introduce the development and application of collagen microspheres embedded with magnetic components, termed "collagen–magnetic particle composite microbeads (CMPMBs)", as innovative tools for cell transplantation. Previous studies have extensively explored nanosized magnetic particles coated with biocompatible polymers, such as dextran-coated magnetic nanoparticles [31], for applications in thermotherapy and magnetic resonance imaging (MRI). One study primarily focused on the specific absorption rate and biocompatibility of magnetic nanoparticles coated with human-like collagen proteins [32], highlighting the significance of surface coatings for hyperthermia and MRI application. Additionally, other studies have reported the use of magnetic nanoparticles coated with hydrolyzed collagen as a novel method for rapidly capturing pathogens [33].

In contrast, our study emphasized the application of CMPMBs in cell transplantation. We specifically explored microcarriers with submicron-sized magnetic particles for enhanced cell-loading capacity and responsiveness to magnetic fields. This approach differentiates our work from previous studies on nano-sized magnetic particles coated with biocompatible polymers. Owing to the requirement for cell attachment, we focused on larger collagen magnetic particles, which are approximately 1000 times larger than conventional medical magnetic particles. These composite microspheres, which incorporate magnetic components within a collagen matrix, were designed to function as both scaffolds and actuating elements capable of remote manipulation. This dual functionality enables precise spatial control over cell transplantation and the potential for targeted drug delivery facilitated by external magnetic field modulation. Additionally, the capacity to induce cellular responses through thermal and mechanical stimuli via magnetic actuation offers novel therapeutic intervention opportunities.

The application of micro-sized collagen–magnetic particle composites extends beyond scaffold engineering, presenting methodological breakthroughs in the construction of artificial organs and the development of efficient bioreactors that closely replicate natural organ environments. Natural organs involve complex interactions between various cell types positioned in defined locations, necessitating advanced technologies for superior cell trafficking and multicellular co-cultures. Our proposed use of magnets to position collagen–magnetic particle composite microbeads as cell carriers represents a pioneering solution for accurately positioning and targeting cells to the desired locations. This innovation paves the way for the creation of complex multicellular constructs that closely mimic the structure of natural organs.

This study emphasizes the capability of precise spatial placement and manipulation using magnets, which is essential for effective cell transplantation. Our primary objective was to demonstrate the effectiveness of these nanoparticles as cell carriers. While we briefly addressed cell transport capabilities, we did not discuss the medical effectiveness of these particles, such as transplantation success rates and toxicity evaluations, which are crucial for practical applications. The focus of our investigation was to elucidate the fundamental relationship between collagen concentration and particle size, thereby providing detailed insights into the preparation of these particles, which is critical for advancements in this field. Additionally, we examined the impact of particle surface roughness on particle size distribution, as this parameter significantly influences cell interactions and behavior.

Our aim is to uncover the potential of CMPMBs as carriers for cells, thereby transforming approaches to targeted drug delivery and tissue regeneration. This study not only seeks to offer innovative solutions to complex medical challenges but also aims to lay the foundation for future advancements in the synthesis and application of biomaterial composites.

2. Materials and Methods

2.1. Materials

Type I porcine collagen (1 wt%) treated with pepsin was obtained from Nippon Ham Foods Co., Ltd. (Osaka, Japan). Carbonate buffer (pH 10.02) was purchased as a standard solution powder reagent from DKK-TOA Co. Ltd. (Tokyo, Japan). Iron (II,III) oxide powder

(<5 μm, 95%) was acquired from Merck. Ethanol (99.5%), fluorescein isothiocyanate (FITC), and acetic acid (0.1 mol/L) were procured from FUJIFILM Wako Pure Chemical Co. (Osaka, Japan).

2.2. Preparation of CMPMBs

To prepare the CMPMBs (see Figure S1), Type I porcine collagen was diluted using 0.01 M acetic acid to achieve concentrations of 0.25, 0.50, 0.75, and 1.0 wt%. The resulting solutions, with a total volume of 10 mL each, were stirred at room temperature until they were fully dissolved. Subsequently, 0.25 g of iron oxide powder was dispersed into 10 mL of collagen solution under continuous stirring at 500 rpm for 30 min at 4 °C. This process was conducted to ensure homogeneity. The collagen–iron oxide mixtures were transferred to a spray container and sprayed onto a Teflon sheet (500 × 500 × 1 mm, AS ONE Co., Ltd., Osaka, Japan) from a height of 15 cm using a 25 mL spray bottle (Φ24 × 100 mm, MonotaRO Co., Ltd., Osaka, Japan). The sprayed sheets were exposed to UV irradiation using a UV light source (UV Lamp 4, 8 W, Camag, Muttenz, Switzerland) for 15 min to crosslink collagen. After UV exposure, the sheets were immersed in ethanol and sonicated using an ultrasonic device (120KAL, Mr. Sonic Cleaner Co., Ltd., Tokyo, Japan) to detach the CMPMBs from the Teflon sheets. The particles precipitated in the ethanol solution were collected and dried at room temperature for 1 d.

2.3. Fluorescence Microscopy

FITC staining was used to visualize the collagen in the prepared particles. A stock solution of FITC was prepared by dissolving 3 mg of FITC powder in 1.5 mL of ethanol to obtain a concentration of 2 mg/mL. A total of 100 μL of this FITC solution was added to the dried CMPMBs and incubated for 10 min at room temperature in the dark. After incubation, the particles were allowed to spontaneously sediment for 1 h, and the supernatant containing unbound FITC was discarded. The particles were then resuspended in 10 mL of distilled water and allowed to stand for 24 h to ensure the complete removal of any remaining unbound dye. This rinsing process was repeated three times. As a control, the same staining and rinsing procedure was performed on iron (II,III) oxide powder to assess the non-specific binding of FITC. The stained CMPMBs and control Fe_3O_4 powder were then mounted on glass slides and observed under a fluorescence microscope (Leica DMI3000 B; Leica Microsystems, Wetzlar, Germany) equipped with a filter set for FITC (excitation wavelength: 480 nm, emission wavelength: 527 nm). Images were captured using a digital camera (Nikon D50; Nikon Corporation, Tokyo, Japan) with consistent exposure settings for both the samples.

2.4. Scanning Electron Microscopy (SEM)

For the SEM analysis, a CMPMB suspension was prepared by dispersing the particles in ethanol. A small volume of this suspension was then carefully dropped onto an aluminum foil substrate. The substrate containing the sample droplets was subsequently placed in a refrigerator maintained at 4 °C for 24 h. This slow-drying process was intended to minimize particle aggregation. After drying, the particles that adhered to the aluminum foil were mounted onto SEM stubs using conductive carbon tape to ensure electrical continuity. The samples were sputtered with Pt/Pd (JFC-1600, JEOL Ltd., Tokyo, Japan) before the SEM analysis. The coated samples were analyzed using a JEOL JSM-6510 scanning electron microscope. The SEM images were captured at an accelerating voltage of 15 kV under high-vacuum conditions. The analysis included magnifications ranging from 500× to 10,000× magnification.

2.5. Viscosity Measurement

The viscosities of the aqueous collagen solutions at different concentrations were measured using a Brookfield DV-II+ programmable viscometer (Middletown, MA, USA) equipped with a 48 mm parallel plate spindle. For each measurement, 4 mL of the collagen solution was loaded into the sample chamber, and the viscosity was measured at 25 °C

with a rotational speed of 0.01 rpm, corresponding to a shear rate of approximately 1.4 s^{-1}. The viscometer was calibrated using standard viscosity reference fluids before measurements. The reported viscosity values were calculated as the average of three independent measurements for each concentration of collagen.

2.6. Adsorption and Desorption Test of CMPMBs

A custom-made polystyrene container (80 mm long diameter, 50 mm short diameter) with a 2 cm high rim was prepared. The bottom of the container was sealed with a 10 μm thick polyvinylidene chloride film (Saran Wrap: Asahi Kasei Co. Ltd., Tokyo, Japan). A suspension of CMPMBs (2 mL) in distilled water was poured into the container. An ultra-thin alumina ceramic plate (50 mm × 30 mm × 0.1 mm, KA6, Kyoritsu Elex, Saga, Japan) was used as the base for the adsorption and desorption tests. Stainless steel foil strips (40 mm long, 2 mm wide, 10 μm thick, SUS403, The Nilaco Corp., Japan) were attached to the ceramic plate at 1 cm intervals using a silicone adhesive (TSE397-C, Momentive Performance Materials Japan LLC, Gunma, Japan). Neodymium magnetic sheet strips (20 mm long, 2 mm wide, 0.4 mm thick, Shinkyo Corp., Tokyo, Japan) were magnetically attached to the backside of the second, fourth, and fifth stainless steel foil strips from the left. To test the adsorption, the magnetic strip-attached ceramic plate was brought into contact with the polyethylene film bottom of the container holding the particle suspension. After a contact time of 10 s, the plate was pulled away from the container to test the desorption of the particles from the magnetic regions (Figure S2). The adsorption and desorption behaviors of the CMPMBs on the magnetic and non-magnetic regions of the plate were visually observed and recorded using a digital camera.

2.7. Evaluation of Positioning Accuracy of CMPMBs on Magnetic Sheet

To evaluate the positioning accuracy of the CMPMBs on a neodymium magnetic sheet, the following method was employed. A neodymium magnetic sheet (1 cm long × 2 mm wide) was immersed in a well-dispersed aqueous suspension of CMPMBs. The suspension consisted of 10 mL of distilled water with a particle concentration of 1 mg/mL. After a brief immersion period of 3 s, which was optimized to maximize the surface interaction without oversaturation, the sheets were subjected to an ultrasonic cleaning process (40 kHz, 200 W) for 30 min to remove loosely adherent particles. This step ensures that only the particles strongly bound to the magnetic sheets remained attached. The adsorption of the CMPMBs on the magnetic sheet was carefully observed using an optical microscope (Leica DMI3000 B; Leica Microsystems, Wetzlar, Germany) at a magnification of 2.5×. The captured images were processed and analyzed using ImageJ (ver.1.54 h), an open-source image analysis software (National Institutes of Health, Bethesda, MD, USA). The software was used to quantify the flatness of the magnetic sheet surface to which the CMPMBs were attached (Figure S3 illustrates the image-processing procedure for processing the image). Through this analysis, the surface roughness parameters, arithmetic average roughness (Ra), and maximum height roughness (Rz) were determined. Ra and Rz were calculated using the following equations [34]:

$$\mathrm{Ra} = \frac{1}{L}\int_0^L |Z(x)|\mathrm{d}x, \quad \mathrm{Rz} = z_{\max} - z_{\min}$$

where L is the measurement length and $Z(x)$ represents the height of the profile. $z_{\max}$ is the highest point, and $z_{\min}$ is the lowest point within the measurement interval. These measurements are important for evaluating the influence of the size distribution properties of CMPMBs on the positioning accuracy of the magnetic sheets.

2.8. Utility Test of CMPMBs as Cellular Transport Carrier: Cell Culture and Monitoring

Mouse fibroblast NIH/3T3 cells were obtained from JCRB (Osaka, Japan). The cells were cultured in RPMI-1640 medium (Fujifilm, Tokyo, Japan) containing 10% fetal bovine serum (Nichirei Bioscience, Tokyo, Japan), 100 μg/mL streptomycin, and 100 μg/mL

penicillin. All cells were cultured at 37 °C, 5% CO_2. To facilitate the adhesion of cells to the CMPMBs, approximately 0.1 g of CMPMBs and 4 mL of culture medium containing 20 × 105 NIH/3T3 cells were combined in a conical tube and incubated without disturbance for 6 h. Following the described treatment, the CMPMBs with adherent NIH/3T3 cells were transferred to an ultra-thin ceramic membrane (KA6, Kyoritsu Elex, Saga, Japan) and seeded across its surface. This ceramic membrane, now bearing CMPMBs with adherent NIH/3T3 cells, was placed in a 6 cm diameter plastic dish, which was then filled with 4 mL of culture medium. After an additional 48 h cultivation period, the samples were fixed in 10% formalin and subsequently stained with hematoxylin and eosin (H&E).

3. Results and Discussion

3.1. Light Microscopy and Fluorescence Microscopy

The presence of collagen in the synthesized magnetic particles was confirmed using optical and fluorescence microscopy. Figure 1 shows (a) a brightfield image and (b) a fluorescence microscopy image of the CMPMBs stained with fluorescein isothiocyanate (FITC). Please note that these CMPMBs are considerably larger than submicron-sized magnetic particles because they incorporate collagen, which forms a matrix around them. The fluorescence signal from the FITC stain covered the entire surface of the prepared particles, indicating the presence of collagen throughout the particles. In contrast, the control sample of iron oxide particles (Figure 1c,d) did not exhibit any fluorescence, confirming the specificity of FITC staining for collagen. The similarity in the particle profile between the brightfield and fluorescence images demonstrated that the collagen-embedded magnetic particles were uniformly covered by collagen. The synthesized collagen–magnetic particles had diameters of less than 5 μm and could be dispersed in distilled water. However, the magnetic particles were trapped within the collagen aggregates, suggesting that collagen acted as a binder for the magnetic particles while simultaneously embedding them. This unique structure of CMPMBs is expected to provide enhanced biocompatibility and stability for biological applications.

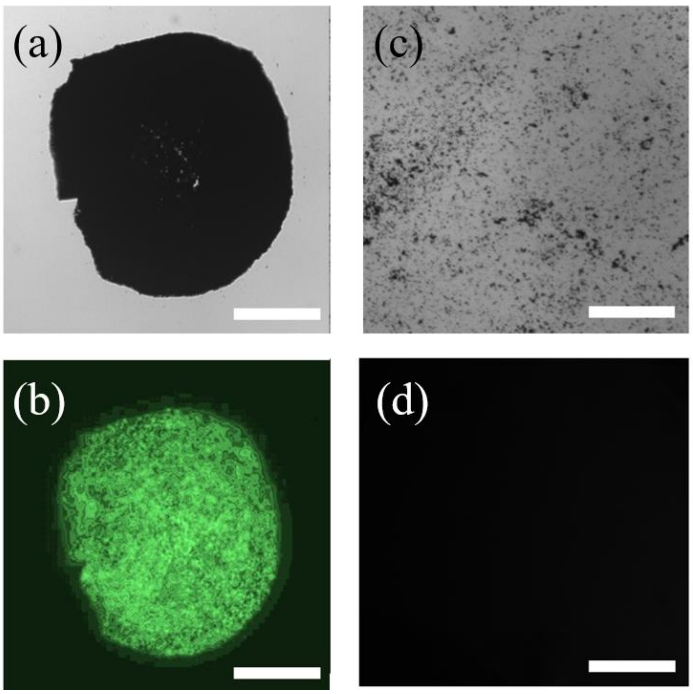

Figure 1. Microscopic images of CMPMB and magnetic particle without collagen. (**a**,**b**) Brightfield and fluorescence microscopy images, respectively, of a FITC-treated CMPMB. (**c**,**d**) Corresponding brightfield and fluorescence microscopy images of a FITC-treated magnetic particle without collagen compositing. Scale bars: 100 μm.

3.2. SEM

SEM analysis revealed distinct morphological features between the CMPMBs and powdered iron oxide. Figure 2 presents SEM images of the collagen–magnetic particles and powdered iron oxide (Fe_3O_4). The surface morphology of the collagen–magnetic particles exhibited an uneven structure with smooth protrusions formed by particles approximately 0.3 μm in size (Figure 2a). In contrast, the pure iron oxide particles displayed a more distinct and uniform particle diameter of 0.3 μm (Figure 2b). The smoothness of the uneven structure in the CMPMBs became more pronounced with increasing collagen concentration. This suggests that the smoothing of the 0.3 μm scale unevenness can be attributed to the covering of the iron oxide particles by collagen.

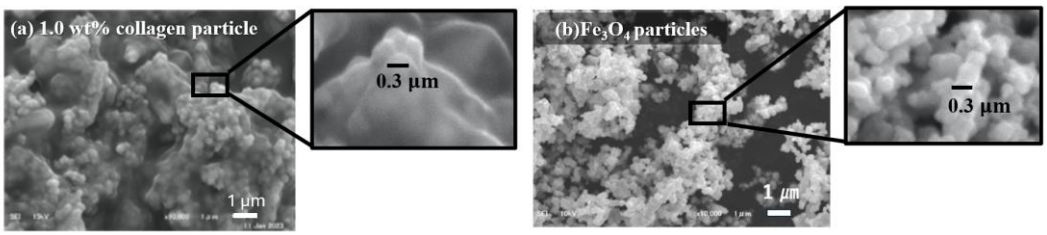

Figure 2. SEM images: (**a**) CMPMBs prepared with 1 w% collagen concentration; (**b**) iron oxide particles without collagen. The subheading images at the right side of each image show the enlarged image of the framed areas.

The fact that the morphology of collagen–magnetic particles is dominated by the shape of the magnetic particles implies that the surface morphology of the cells can be controlled by the shape characteristics of the magnetic microparticles. It is also noteworthy that the degree of uneven smoothing can be adjusted by varying the collagen concentration. Based on the knowledge that the surface morphology of scaffolds directly influences cell morphology [35,36], migration [37,38], and, ultimately, cell proliferation [39,40], this surface control tool is crucial for optimizing cell adhesion and proliferation. It is also important to note that not only the size but also the morphological shape of magnetic nanoparticles play a crucial role in determining their magnetic response and positioning accuracy when used as cell carriers. While our study focused on spherical iron oxide particles, previous research has shown that alternative morphologies, such as rod-shaped [41] or cubic [42] nanoparticles, can exhibit lower magnetic responses than their spherical counterparts. This can be attributed to the shape anisotropy of nonspherical particles, which influences their magnetic properties and interactions with external magnetic fields.

3.3. Relationship between Particle Size of CMPMBs and Viscosity of Collagen Solution Used in Their Preparation

Particle size is important for controlling positioning accuracy when particles are used as cell carriers. Controlling the particle size is also important for controlling the resistance and driving force of the cell carrier particles when they are magnetically moved. In this section, we discuss the effect of collagen concentration on particle size. Figure 3a–d show the size distribution of the CMPMBs obtained at different collagen concentrations. The average particle diameters were 64 ± 56, 150 ± 110, 360 ± 150, and 410 ± 160 μm at collagen concentrations of 0.25, 0.5, 0.7, and 1.0 wt%. With increasing collagen concentration, the particle size increased, and the size distribution became polydisperse. Figure 3e shows the relationship between the average particle size, collagen concentration, and viscosity of the collagen solution. The dependence of the average particle size on the collagen concentration was similar to that of the viscosity of the collagen solution used in the preparation. This finding implies that the particle size is determined by viscosity in this range of preparation environments. These results suggest that viscosity or collagen concentration is a determinant controlling the size of CMPMBs. Next, the effect of the solution viscosity on the particle size is discussed by considering the spray situation, that is, the behavior of the viscous liquid when shear stress is applied to the liquid. The atomizer breaks the liquid into fine droplets in

the following steps. When a liquid under high pressure is forced through the narrow orifice of a nebulizer and released into the atmosphere, the pressure decreases rapidly. This pressure drop creates a shear force on the surface of the liquid, which tears it apart and splits it into fine droplets. In this case, the relationship between the droplet diameter d and viscosity of the liquid can be explained using the Weber number We, which is a dimensionless number expressing the ratio of the inertial force to the surface tension of the liquid, and the Reynolds number Re, which is a dimensionless number expressing the ratio of the inertial force to the viscous force, as follows.

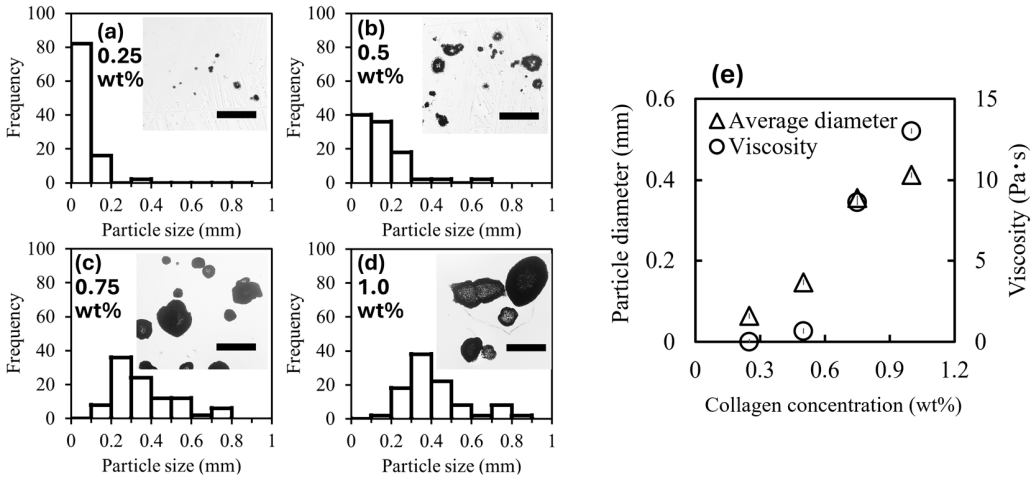

Figure 3. Analysis of magnetic collagen particle size and viscosity dependence. (**a**–**d**) Size distribution of collagen particles, determined from optical microscope images. The figure insets show typical images of magnetic collagen particles at different collagen concentrations, indicated in the upper-left corner of each inset. Scale bars: 0.5 mm. (**e**) Relationship between the collagen concentration and both the viscosity of the collagen solution used and the average diameter of the magnetic collagen particles formed.

From the definitions of the Weber number (We) and Reynolds number (Re),

$$\mathrm{We} = \rho v^2 d/\sigma,\ \mathrm{Re} = \rho v d/\mu$$

where ρ is the density of the liquid [kg/m^3], v is the relative velocity of the liquid [m/s], d is the characteristic length (droplet diameter) [m], and σ is the surface tension of the liquid [N/m]. Combining these equations to express the droplet diameter d, we obtain the following:

$$d = (\mathrm{We} \cdot \mu)/(\rho v) \ = \ \left(\mathrm{We} \cdot \mu^2\right)/(\rho \cdot \mathrm{Re} \cdot \sigma)$$

From this equation, we can observe that the droplet diameter d is proportional to the viscosity of the liquid μ and inversely proportional to the density ρ and relative velocity v. However, in a real atomizer, other factors, such as nozzle shape and pressure difference, also affect the droplet size; therefore, these factors must also be considered.

3.4. Adsorption and Desorption Test of CMPMBs on Magnetic Sheets

Our goal was to construct a system that enables cells to move into and out of the designed spaces using magnetic force by using our cell-loaded CMPMB as a cell carrier. In this section, we tested the attachment and detachment of our CMPMBs to areas of the magnetic sheet by using an ultra-thin ceramic plate equipped with a detachable magnetic sheet strip on the back to verify whether the magnetic force can be used to place the CMPMBs in the desired spaces (see Supplementary Movie S1 for a video of this experiment).

Figure 4 illustrates the behavior of the CMPMB suspension in contact with the ultra-thin ceramic plate when a detachable magnetic sheet strip was attached to the back of the plate and when the magnetic sheet strip was removed. Figure 4a shows the CMPMB suspension just before the magnetic sheet strip was attached to the ceramic plate, and

Figure 4b shows the suspension 30 s after the magnetic sheet strip was attached. When the magnetic sheet strips were applied to the ceramic plate, the CMPMBs in the suspension clustered in the areas where the magnetic sheet strips were located. This behavior indicated that the CMPMBs were magnetic and could be arranged according to the pattern of the designed area (magnetic sheet).

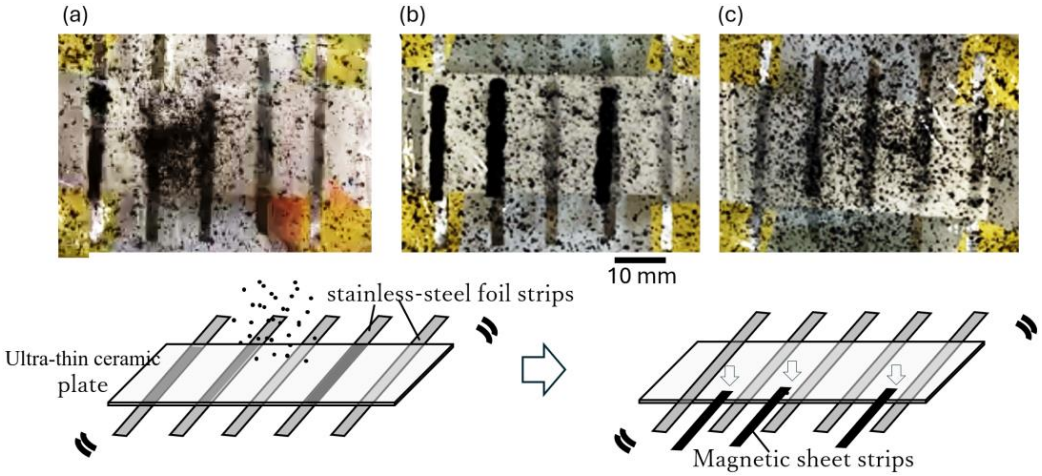

Figure 4. Adsorption and desorption dynamics of CMPMBs on magnetic sheet strips. (**a**) Image captured before attaching the magnetic sheet strip to the bottom of the plastic film in a container filled with the particle suspension. (**b**) Image taken approximately 30 s following the attachment of the magnetic sheet strip to the bottom of the container, demonstrating initial adsorption dynamics. (**c**) Image after the magnetic sheet strip was removed from the plastic film and the container was shaken, illustrating the desorption characteristics of the magnetic particles.

To demonstrate detachment of the CMPMBs, the magnetic sheet strip was physically removed from the ceramic plate. As shown in Figure 4c, 1 min after removal of the magnetic sheet strip, the black areas where the magnetic sheet strip was previously attached were diluted and redispersed in the suspension. This observation confirmed that the CMPMBs could be selectively detached from the desired locations.

Furthermore, we found that the CMPMBs could be repositioned to the same areas by reattaching the magnetic sheet strips to the ceramic plate. This reversible attachment and detachment highlight the potential of these CMPMBs as cell carriers that can be placed and removed at designated times and locations through magnetic manipulation.

3.5. Evaluation of Positioning Accuracy of CMPMBs on Magnetic Sheet

In the previous section, we confirmed that the use of removable magnetic sheets allows for CMPMBs to be placed in the designed space and detached from the previous location. To place cells in the designed location, CMPMBs, which are carriers of the cells, must be placed in a restricted space. In fact, the particles adsorbed on the magnetic sheet deviated from the magnetic sheet contour (see upper images of Figure 5a). To minimize the deviation of the CMPMBs from their designed spatial location, this chapter estimated the deviation from the straight line of the edge contour created by the collagen particles adsorbed on the magnetic sheet using surface roughness to clarify how well the collagen particles were placed at the intended location. Here, we evaluated the effect of collagen particles prepared at different concentrations on the deviation from the straight edge.

In this study, we investigated the relationship between the collagen concentration used in the preparation of CMPMBs and the resulting surface roughness when these particles are adsorbed onto the edges of magnets. Figure 5a presents the surface roughness parameters (Ra and Rz) obtained from image analysis of magnet edges adsorbed with CMPMBs prepared from collagen solutions of different concentrations. The graph reveals that the surface roughness increases almost linearly with the collagen concentration.

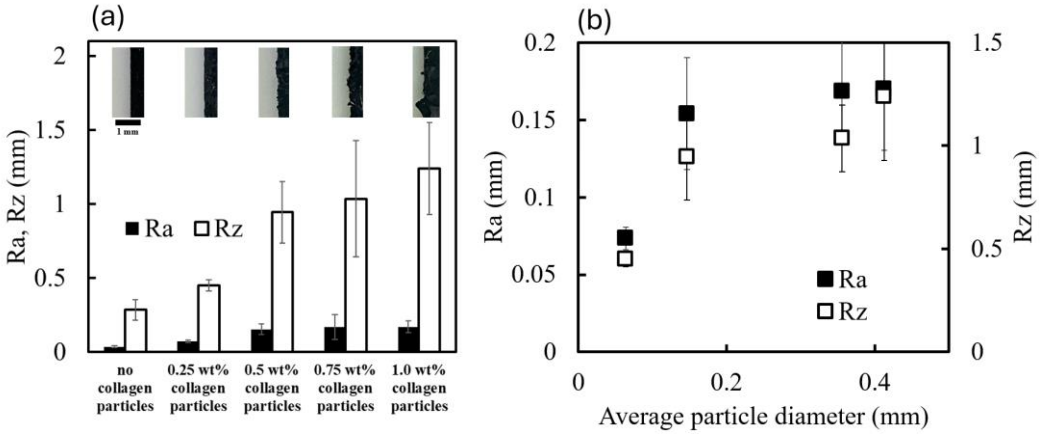

Figure 5. Evaluation of placement accuracy of magnetic collagen particles on a magnetic sheet. (**a**) Top: Magnified images of the edge of the magnetic sheet with adsorbed CMPMBs at different collagen concentrations. Bottom: Corresponding values of the surface roughness parameters Ra and Rz, comparing the edge of the magnetic sheet surface without and with CMPMBs. (**b**) Plot representing the relationship between the average size of the CMPMBs and the surface roughness parameters Ra and Rz.

To further understand the relationship between particle size and surface roughness, Ra and Rz were plotted against the average particle diameter (Figure 5b). The results show that Ra and Rz increase linearly up to a particle diameter of approximately 0.2 mm. This observation is consistent with the theoretical calculation of the average surface roughness (Ra) of a one-dimensional array of spherical particles, where Ra is directly proportional to the radius (r) of the spheres.

However, when the particle diameter exceeds 0.2 mm, the rate of increase in roughness becomes moderate, deviating from the predicted linear relationship. We propose that this deviation is due to the increasing polydispersity of the particle size distribution as the collagen concentration and, consequently, the average particle size increase. As evident from the particle size distributions shown in Figure 3a,b, CMPMBs prepared in high collagen concentration solutions exhibit a more polydisperse size distribution.

The relationship between surface roughness and average particle size is significantly different for a system consisting of polydisperse collagen particles compared to a system composed of monodisperse particles of the same size (r). In a polydisperse system, smaller particles can occupy the spaces between larger particles, resulting in a more compact arrangement and a lower surface roughness than predicted by the theoretical calculation for monodisperse particles.

This finding has important implications for the precise placement of CMPMBs in desired locations. Even when using larger particles with a polydisperse size distribution, it is possible to achieve accurate positioning of the particles because of the space-filling effect of the smaller particles. This suggests that the use of CMPMBs prepared from high collagen concentration solutions, which have a larger average size and a more polydisperse size distribution, may be advantageous for applications that require precise spatial control.

3.6. Utility of CMPMBs as a Cell Carrier

We evaluated the effectiveness of CMPMBs as cellular transport carriers. Figure 6 illustrates that blackish CMPMBs were visible on the ceramic membrane, with a surrounding distribution of cells. These are NIH3T3 cells, which migrate from and proliferate around the CMPMBs. This observation suggests that CMPMBs function not only as a cellular scaffold but also a safe transport for living cells and facilitate their distribution in the vicinity of the particles post-migration.

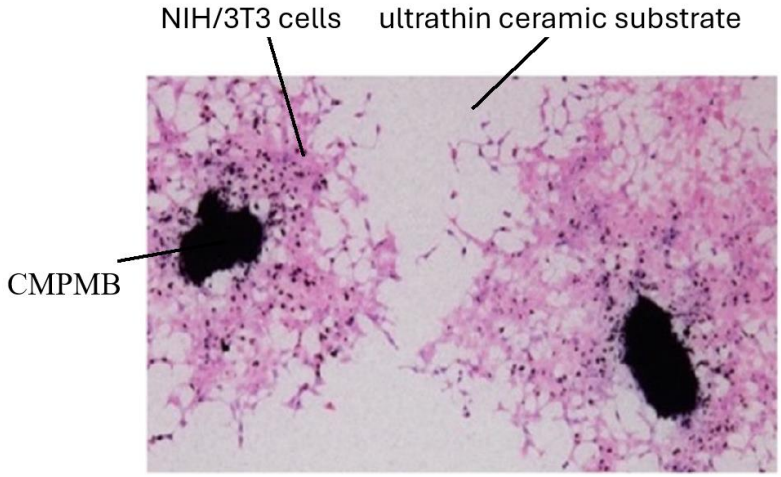

Figure 6. NIH/3T3 cells adhering to and migrating around CMPMBs seeded on an ultrathin ceramic substrate. After 48 h of culture, the dark particles are clearly visible on the membrane, with surrounding cells migrating away from these centers. The sample was stained using Hematoxylin and Eosin (H&E).

Further investigation is necessary to fully elucidate the potential of our cell carriers for manipulation via a magnetic field. This includes examining the precision of cell placement, capacity for desorption of the CMPMBs following incubation, and ability of these particles to bind cells in predetermined locations through magnetic field manipulation. Although this study demonstrated the successful adhesion and proliferation of NIH/3T3 fibroblasts on CMPMBs, the effects of particle size and surface roughness on cell adhesion and proliferation were not explicitly explored. These particle properties, which can be tuned by adjusting collagen concentration, are known to play a significant role in regulating cellular responses. Future studies should systematically investigate the relationship between particle characteristics and cell behavior to optimize the performance of CMPMBs as cell carriers and scaffolds for tissue-engineering applications.

Additionally, we acknowledge that cell type specificity has not been explicitly addressed. Although collagen is a generally favorable substrate for various cell types, future studies should explore the functionalization of CMPMBs with cell-specific ligands or peptides to enhance their targeting capabilities for specific cell types and applications. This could involve the incorporation of cell-adhesive peptide sequences, growth factors, or antibodies that promote selective adhesion and growth of the desired cell populations. Such functionalization strategies could expand the utility of CMPMBs as targeted cell-delivery vehicles for a range of tissue engineering and regenerative medicine applications.

4. Conclusions

This study successfully developed and characterized collagen–magnetic particle composite microbeads (CMPMBs) as promising platforms for targeted cell delivery and tissue engineering applications. The particles, prepared by combining iron oxide powder with collagen solutions, exhibited a distinct concavo-convex morphology that differed from the smooth surface of the pure iron oxide particles. The average particle diameter increased with collagen concentration, closely correlating with the viscosity of the collagen solution, providing a valuable tool for controlling particle size and surface morphology for optimal cell adhesion and proliferation. Adsorption and desorption tests demonstrated the ability to selectively position and detach particles using removable magnetic sheet strips, highlighting the potential for the precise spatial control of cell carriers. Surface roughness analysis revealed a linear relationship between the roughness and particle size up to a certain collagen concentration, which has implications for accurate particle positioning. Cell culture experiments confirmed the utility of CMPMBs as effective cell carriers, with keratinocytes successfully adhering to and proliferating around the particles, underscoring their potential as scaffolds for cell growth and migration.

Future studies should focus on the precision of cell placement, desorption of particles following incubation, and the ability to bind cells in predetermined locations through magnetic field manipulation. Additionally, investigations on the functionalization of CMPMBs with cell-specific ligands or peptides could enhance their targeting capabilities for specific cell types and applications. These investigations will fully explore the capabilities of CMPMBs as cell carriers and their potential for manipulation using magnetic fields in tissue engineering and regenerative medicine.

Supplementary Materials: The following supporting information can be downloaded at: https://www.mdpi.com/article/10.3390/macromol4030027/s1, Figure S1: Schematic diagram of the steps in the procedure for obtaining collagen–magnetic particle composite microbeads (CMPMBs); Figure S2: Schematic diagram of the steps in the adsorption/desorption test of CMPMBs on a magnetic sheet.; Figure S3: Procedure for processing images; Movie S1: Video of adsorption and desorption test of CMPMBs on magnetic sheets.

Author Contributions: Conceptualization, S.A., Y.O. and T.N.; methodology, T.N.; formal analysis, D.T. and S.I.; investigation, D.T., S.A. and S.I.; resources, A.K. and S.A.; data curation, D.T., T.N. and S.I.; writing—original draft preparation, T.N.; writing—review and editing, T.N., S.A, Y.O. and A.K.; visualization, T.N. and S.I.; supervision, T.N.; project administration, Y.O.; funding acquisition, T.N. All authors have read and agreed to the published version of the manuscript.

Funding: This work was supported by JSPS (Japan Society for the Promotion of Science) KAKENHI under grant number 22K12821.

Data Availability Statement: Data are contained within the article and Supplementary Materials.

Acknowledgments: The SEM was conducted at the Analytical Research Center for Experimental Sciences, Saga University. These research instruments were supported by the Ministry of Education, Culture, Sports, Science and Technology of Japan (MEXT) through the Advanced Research Infrastructure Sharing Promotion Program (Support Program for Introduction of New Shared Systems) under grant number JPMXS0422400020.

Conflicts of Interest: The authors declare no conflicts of interest.

References

1. Karamanos, N.K.; Theocharis, A.D.; Piperigkou, Z.; Manou, D.; Passi, A.; Skandalis, S.S.; Vynios, D.H.; Orian-Rousseau, V.; Ricard-Blum, S.; Schmelzer, C.E.H.; et al. A guide to the composition and functions of the extracellular matrix. *FEBS J.* **2021**, *288*, 6850–6912. [CrossRef] [PubMed]
2. Huang, J.; Zhang, L.; Wan, D.; Zhou, L.; Zheng, S.; Lin, S.; Qiao, Y. Extracellular matrix and its therapeutic potential for cancer treatment. *Signal Transduct. Target. Ther.* **2021**, *6*, 153. [CrossRef]
3. Karamanos, N.; Ricard-Blum, S.; Kletsas, D. Extracellular matrix: The dynamic structural and functional network in health and disease. *IUBMB Life* **2022**, *74*, 926. [CrossRef]
4. Rao, Z.; Lin, Z.; Song, P.; Quan, D.; Bai, Y. Biomaterial-based Schwann cell transplantation and Schwann cell-derived biomaterials for nerve regeneration. *Front. Cell. Neurosci.* **2022**, *16*, 926222. [CrossRef] [PubMed]
5. Barberio, C.; Saez, J.; Withers, A.; Nair, M.; Tamagnini, F.; Owens, R.M. Conducting polymer-ECM scaffolds for human neuronal cell differentiation. *Adv. Healthc. Mater.* **2022**, *11*, 2200941. [CrossRef] [PubMed]
6. Reddy, M.S.B.; Ponnamma, D.; Choudhary, R.; Sadasivuni, K.K. A comparative review of natural and synthetic biopolymer composite scaffolds. *Polymers* **2021**, *13*, 1105. [CrossRef]
7. Echeverria Molina, M.I.; Malollari, K.G.; Komvopoulos, K. Design challenges in polymeric scaffolds for tissue engineering. *Front. Bioeng. Biotechnol.* **2021**, *9*, 617141. [CrossRef] [PubMed]
8. Wang, S.; Hashemi, S.; Stratton, S.; Arinzeh, T.L. The effect of physical cues of biomaterial scaffolds on stem cell behavior. *Adv. Healthc. Mater.* **2021**, *10*, 2001244. [CrossRef]
9. Meesane, J. Mimicked Molecular Structures in Scaffolds. In *Mimicked Tissue Engineering Scaffolds for Maxillofacial and Articular Cartilage Surgery*; Springer: Berlin/Heidelberg, Germany, 2022; pp. 47–61.
10. Salvatore, L.; Gallo, N.; Natali, M.L.; Terzi, A.; Sannino, A.; Madaghiele, M. Mimicking the hierarchical organization of natural collagen: Toward the development of ideal scaffolding material for tissue regeneration. *Front. Bioeng. Biotechnol.* **2021**, *9*, 644595. [CrossRef]
11. Zhu, J.; Li, Z.; Zou, Y.; Lu, G.; Ronca, A.; D'Amora, U.; Liang, J.; Fan, Y.; Zhang, X.; Sun, Y. Advanced application of collagen-based biomaterials in tissue repair and restoration. *J. Leather Sci. Eng.* **2022**, *4*, 30. [CrossRef]

12. Zheng, M.; Wang, X.; Chen, Y.; Yue, O.; Bai, Z.; Cui, B.; Jiang, H.; Liu, X. A review of recent progress on collagen-based biomaterials. *Adv. Healthc. Mater.* **2023**, *12*, 2202042. [CrossRef] [PubMed]
13. Wang, Y.; Wang, Z.; Dong, Y. Collagen-based biomaterials for tissue engineering. *ACS Biomater. Sci. Eng.* **2023**, *9*, 1132–1150. [CrossRef]
14. Copes, F.; Pien, N.; Van Vlierberghe, S.; Boccafoschi, F.; Mantovani, D. Collagen-based tissue engineering strategies for vascular medicine. *Front. Bioeng. Biotechnol.* **2019**, *7*, 166. [CrossRef]
15. Capella-Monsonís, H.; De Pieri, A.; Peixoto, R.; Korntner, S.; Zeugolis, D.I. Extracellular matrix-based biomaterials as adipose-derived stem cell delivery vehicles in wound healing: A comparative study between a collagen scaffold and two xenografts. *Stem Cell Res. Ther.* **2020**, *11*, 510. [CrossRef]
16. Plouffe, B.D.; Murthy, S.K.; Lewis, L.H. Fundamentals and application of magnetic particles in cell isolation and enrichment: A review. *Rep. Prog. Phys.* **2014**, *78*, 016601. [CrossRef]
17. Pastucha, M.; Farka, Z.; Lacina, K.; Mikušová, Z.; Skládal, P. Magnetic nanoparticles for smart electrochemical immunoassays: A review on recent developments. *Microchim. Acta* **2019**, *186*, 312. [CrossRef] [PubMed]
18. Van Durme, R.; Crevecoeur, G.; Dupré, L.; Coene, A. Model-based optimized steering and focusing of local magnetic particle concentrations for targeted drug delivery. *Drug Deliv.* **2021**, *28*, 63–76. [CrossRef] [PubMed]
19. Cai, K.; Luo, Z.; Hu, Y.; Chen, X.; Liao, Y.; Yang, L.; Deng, L. Magnetically Triggered Reversible Controlled Drug Delivery from Microfabricated Polymeric Multireservoir Devices. *Adv. Mater.* **2009**, *21*, 4045–4049. [CrossRef]
20. Gao, J.; Gu, H.; Xu, B. Multifunctional Magnetic Nanoparticles: Design, Synthesis, and Biomedical Applications. *Acc. Chem. Res.* **2009**, *42*, 1097–1107. [CrossRef]
21. Namdeo, M.; Saxena, S.; Tankhiwale, R.; Bajpai, M.; Mohan, Y.M.; Bajpai, S.K. Magnetic nanoparticles for drug delivery applications. *J. Nanosci. Nanotechnol.* **2008**, *8*, 3247–3271. [CrossRef]
22. Kuhara, M.; Takeyama, H.; Tanaka, T.; Matsunaga, T. Magnetic Cell Separation Using Antibody Binding with Protein a Expressed on Bacterial Magnetic Particles. *Anal. Chem.* **2004**, *76*, 6207–6213. [CrossRef] [PubMed]
23. Shi, D.; Sadat, M.E.; Dunn, A.; Mast, D. Photo-Fluorescent and Magnetic Properties of Iron Oxide Nanoparticles for Biomedical Applications. *Nanoscale* **2015**, *7*, 8209–8232. [CrossRef]
24. Kaushik, S.; Thomas, J.; Panwar, V.; Ali, H.; Chopra, V.; Sharma, A.; Tomar, R.; Ghosh, D. In Situ Biosynthesized Superparamagnetic Iron Oxide Nanoparticles (SPIONS) Induce Efficient Hyperthermia in Cancer Cells. *ACS Appl. Bio Mater.* **2020**, *3*, 779–788. [CrossRef]
25. Sionkowska, A.; Grabska, S. Preparation and characterization of 3D collagen materials with magnetic properties. *Polym. Test.* **2017**, *62*, 382–391. [CrossRef]
26. Wright, A.L.; Righelli, L.; Broomhall, T.J.; Lamont, H.C.; El Haj, A.J. Magnetic nanoparticle-mediated orientation of collagen hydrogels for engineering of tendon-mimetic constructs. *Front. Bioeng. Biotechnol.* **2022**, *10*, 797437. [CrossRef] [PubMed]
27. Zhang, N.; Lock, J.Y.; Sallee, A.; Liu, H. Magnetic Nanocomposite Hydrogel for Potential Cartilage Tissue Engineering: Synthesis, Characterization, and Cytocompatibility With Bone Marrow Derived Mesenchymal Stem Cells. *Acs Appl. Mater. Interfaces* **2015**, *7*, 20987–20998. [CrossRef] [PubMed]
28. Estévez, M.; Montalbano, G.; Gallo-Cordova, A.; Ovejero, J.G.; Izquierdo-Barba, I.; González, B.; Tomasina, C.; Moroni, L.; Vallet-Regí, M.; Vitale-Brovarone, C.; et al. Incorporation of superparamagnetic iron oxide nanoparticles into collagen formulation for 3D electrospun scaffolds. *Nanomaterials* **2022**, *12*, 181. [CrossRef] [PubMed]
29. Omidinia-Anarkoli, A.; Boesveld, S.; Tuvshindorj, U.; Rose, J.C.; Haraszti, T.; Laporte, L.D. An Injectable Hybrid Hydrogel with Oriented Short Fibers Induces Unidirectional Growth of Functional Nerve Cells. *Small* **2017**, *13*, 1702207. [CrossRef]
30. De Paoli, V.M.; De Paoli Lacerda, S.H.; Spinu, L.; Ingber, B.; Rosenzweig, Z.; Rosenzweig, N. Effect of an oscillating magnetic field on the release properties of magnetic collagen gels. *Langmuir* **2006**, *22*, 5894–5899. [CrossRef]
31. Štrbák, O.; Antal, I.; Khmara, I.; Koneracká, M.; Kubovčíková, M.; Závišová, V.; Molčan, M.; Juríková, A.; Hnilicová, P.; Gombos, J.; et al. Influence of Dextran Molecular Weight on the Physical Properties of Magnetic Nanoparticles for Hyperthermia and MRI Applications. *Nanomaterials* **2020**, *10*, 2468. [CrossRef]
32. Chang, L.; Liu, X.L.; Fan, D.; Miao, Y.; Zhang, H.; He, P.; Liu, Q.Y.; Ma, P.; Xue, W.; Luo, Y.; et al. The Efficiency of Magnetic Hyperthermia and in Vivo Histocompatibility for Human-Like Collagen Protein-Coated Magnetic Nanoparticles. *Int. J. Nanomed.* **2016**, *11*, 1175–1185. [CrossRef]
33. Sande, M.G.; Roque, L.; Braga, A.; Marques, M.; Ferreira, D.; Saragliadis, A.; Rodrigues, J.L.; Linke, D.; Ramada, D.; Silva, C.; et al. Design of new hydrolyzed collagen-modified magnetic nanoparticles to capture pathogens. *J. Biomed. Mater. Res. Part B Appl. Biomater.* **2023**, *111*, 354–365. [CrossRef] [PubMed]
34. Gadelmawla, E.S.; Koura, M.M.; Maksoud, T.M.A.; Elewa, I.M.; Soliman, H.H. Roughness parameters. *J. Mater. Process. Technol.* **2002**, *123*, 133–145. [CrossRef]
35. García, M.A.M.; Izadifar, M.; Chen, X. Evaluation of PBS treatment and PEI coating effects on surface morphology and cellular response of 3D-printed alginate scaffolds. *J. Funct. Biomater.* **2017**, *8*, 48. [CrossRef] [PubMed]
36. Czeisler, C.; Short, A.; Nelson, T.; Gygli, P.; Ortiz, C.; Catacutan, F.P.; Stocker, B.; Cronin, J.; Lannutti, J.; Winter, J.; et al. Surface topography during neural stem cell differentiation regulates cell migration and cell morphology. *J. Comp. Neurol.* **2016**, *524*, 3485–3502. [CrossRef]

37. Frost, O.G.; Owji, N.; Thorogate, R.; Kyriakidis, C.; Sawadkar, P.; Mordan, N.; Knowles, J.C.; Lali, F.; Garcia-Gareta, E. Cell morphology as a design parameter in the bioengineering of cell–biomaterial surface interactions. *Biomater. Sci.* **2021**, *9*, 8032–8050. [CrossRef]
38. Gupta, A.; Das, A.; Barui, A.; Das, A.; Chowdhury, A.R. Evaluating the cell migration potential of TiO2 nanorods incorporated in a Ti6Al4V scaffold: A multiscale approach. *J. Mech. Behav. Biomed. Mater.* **2023**, *144*, 105940. [CrossRef]
39. Marques-Almeida, T.; Cardoso, V.F.; Ribeiro, S.; Gama, F.M.; Ribeiro, C.; Lanceros-Mendez, S. Tuning myoblast and preosteoblast cell adhesion site, orientation, and elongation through electroactive micropatterned scaffolds. *ACS Appl. Bio Mater.* **2019**, *2*, 1591–1602. [CrossRef] [PubMed]
40. Khan, M.U.A.; Mehboob, H.; Razak, S.I.A.; Yahya, M.Y.; Yusof, A.H.M.; Ramlee, M.H.; Anand, T.J.S.; Hassan, R.; Aziz, A.; Amin, R. Development of Polymeric Nanocomposite (Xyloglucan-Co-Methacrylic Acid/Hydroxyapatite/SiO2) Scaffold for Bone Tissue Engineering Applications—In-Vitro Antibacterial, Cytotoxicity and Cell Culture Evaluation. *Polymers* **2020**, *12*, 1238. [CrossRef]
41. Marcuello, C.; Chambel, L.; Rodrigues, M.S.; Ferreira, L.P.; Cruz, M.M. Magnetotactic bacteria: Magnetism beyond magnetosomes. *IEEE Trans. Nanobiosci.* **2018**, *17*, 555–559. [CrossRef]
42. Wang, Q.; Ma, X.; Liao, H.; Liang, Z.; Li, F.; Tian, J.; Ling, D. Artificially engineered cubic iron oxide nanoparticle as a high-performance magnetic particle imaging tracer for stem cell tracking. *ACS Nano* **2020**, *14*, 2053–2062. [CrossRef] [PubMed]